SCIENCE CHINA Materials ARTICLES

mater.scichina.com link.springer.com

Published online 5 September 2017 | doi: 10.1007/s40843-017-9090-0
Sci China Mater 2017, 60(9): 811–818

Quantum confinement effect of two-dimensional all-inorganic halide perovskites

Bo Cai[1†], Xiaoming Li[1†], Yu Gu[1†], Moussab Harb[2], Jianhai Li[1], Meiqiu Xie[1], Fei Cao[1], Jizhong Song[1], Shengli Zhang[1], Luigi Cavallo[2] and Haibo Zeng[1*]

ABSTRACT **Quantum confinement effect (QCE), an essential physical phenomenon of semiconductors when the size becomes comparable to the exciton Bohr radius, typically results in quite different physical properties of low-dimensional materials from their bulk counterparts and can be exploited to enhance the device performance in various optoelectronic applications. Here, taking $CsPbBr_3$ as an example, we reported QCE in all-inorganic halide perovskite in two-dimensional (2D) nanoplates. Blue shifts in optical absorption and photoluminescence spectra were found to be stronger in thinner nanoplates than that in thicker nanoplates, whose thickness lowered below ~7 nm. The exciton binding energy results showed similar trend as that obtained for the optical absorption and photoluminescence. Meanwile, the function of integrated intensity and full width at half maximum and temperature also showed similar results, further supporting our conclusions. The results displayed the QCE in all-inorganic halide perovskite nanoplates and helped to design the all-inorganic halide perovskites with desired optical properties.**

Keywords: quantum confinement effect, all-inorganic halide perovskites, nanoplates, temperature dependence luminescence

INTRODUCTION

Over recent years, halide perovskite ABX_3 (ABX_3, A = organic group or alkali cation, B = Pb^{2+}, X = halogen anion) was one of the hottest direct bandgap semiconductors with potential profound optoelectronic applications including solar cells, LEDs, lasers [1–14]. Lots of lower dimensionality perovskites nanocrystals have been reported, because of the advantage of nanotechnology and the mature preparation method and probe equipment [7,9,12,15,16]. Two-dimensional (2D) nanoplate is one of these structures. The research upsurge of 2D halide perovskites in optics have just risen since 2014, due to highly quantum yield, narrow full width at half maximum (FWHM) of photoluminescence, increased exciton binding energy, and reduced fluorescence decay times [15–22]. Recent research showed a strong blue shift in the absorption and photoluminescence (PL) spectra, which indicated a strong quantum confinement effect (QCE) in these structures [15,18,23–25]. The reports for all-inorganic halide perovskites are extremely rare compared to that for the organic-inorganic hybrid halide perovskites. The idea behind this phenomenon is the size of long alkyl chain, which can help the perovskites to form a 2D structure [15,19,26–28]. However, the stability, which is a vital index for application, of all-inorganic halide perovskites is much better than hybrid [7,10,12,29,30]. And the effect of substitution of organic long chain with cesium ions on the QCE with thickness changing is not clear.

In this paper, we considered $CsPbBr_3$ as a typical example, and prepared different $CsPbBr_3$ samples with different thicknesses to obtain the size-dependent QCE. Based on density functional theory (DFT) calculations, we obtain the exciton Bohr diameter of 7 nm for $CsPbBr_3$. With the thickness of the nanoplates reducing, an increasing QCE was identified by bandgaps E_g and exciton binding energy E_b extracted from the absorption spectra. Room temperature PL spectra show a stronger blue shift in 1.8 nm nanoplates than in 3.0 nm nanoplates, indicating a stronger QCE in thinner samples. The in-

[1] MIIT Key Laboratory of Advanced Display Materials and Devices, Institute of Optoelectronics & Nanomaterials, College of Materials Science and Engineering, Nanjing University of Science and Technology, Nanjing 210094, China
[2] King Abdullah University of Science and Technology (KAUST), KAUST Catalysis Center (KCC), Physical Sciences and Engineering Division (PSE), Thuwal 23955-6900, Saudi Arabia
[†] These authors contributed equally to this work.
[*] Corresponding author (email: zeng.haibo@njust.edu.cn)

tegrated intensity *versus* reciprocal of temperature (1/*T*), and FWHM *versus* temperature of temperature dependence PL display similar trend that the thinner sample is, the stronger QCE becomes. This work shows the QCE in all-inorganic halide perovskites and could help to design the all-inorganic halide perovskites with desired optical properties.

EXPERIMENTAL SECTION

Fabrication

Firstly, atomically thin nanoplates were prepared as follows: 0.18 g Cs_2CO_3, 10 mL octadecene (ODE) and 1 mL oleic acid (OA) were mixed in a 3-neck flask, which were degassed under vacuum at 170°C until all the powders were dissolved to form Cs-oleate precursor. Then, 0.735 g $PbBr_2$ was dissolved in 5 mL dimethyl formamide (DMF) combined with 2.5 mL ODE, 0.25 mL OA and 0.25 mL oleylamine (OAm), after which the mixture was stirred for 2 min. Then, 0.2 mL Cs-oleate was added into the mixture under stirring, 0.4 mL $PbBr_2$ precursor was dropped into the stirred mixture. The reaction was quenched by acetone after 1 min. The colloid was centrifuged to remove the unreactive materials in the supernatant, which was finally dispersed in toluene. This resulted in 5 layer nanoplates. To prepare 3 layer nanoplates, additional hydrobromic acid was added (20 μL). Secondly, the thick nanoplates were prepared as follows: 0.3 mL precursor (1 mmol CsBr and 0.5 mmol $PbBr_2$ dissolved in 14 mL dimethylsulfoxide (DMSO) and 1 mL acetic acid (HAc)) and 1.5 mL ligands (1 g octadecaylamine dissolved in 10 mL HAc) were mixed and stirred for 10 min. Then, 5 mL toluene was added and stirred for another 10 min. The reaction was stopped by centrifugation at 6,000 rpm and the precipitation was finally washed two more times and dispersed in 5 mL of toluene.

Measurement and characterization

X-ray diffraction (XRD) patterns were recorded on a multipurpose XRD system D8 Advance from Bruker. UV/vis absorption spectra were obtained using a Shimadzu 3600 UV/vis spectrophotometer and PL spectra were measured with a Varian Cary Eclipse instrument. The temperature dependent PL spectra were measured at Horiba luminescence spectrometer (HR 320) with a laser excitation (442 nm) at different temperatures in a closed-circuit liquid helium system. The light source was focused onto the sample substrate by an immersion-oil objective and the PL signal of single-particle was collected by the same objective and a charge-coupled device camera. Meanwhile, the PL signal was sent through a beam splitter tube to two avalanche photodiodes in a Hanbury Brown-Twiss configuration for the PL decay measurement.

RESULTS AND DISCUSSION

Few-layer $CsPbBr_3$ models and samples

As compared to typical Cd-based quantum dots, halide perovskites have narrower luminescence peaks, broader color gamut, lower cost and higher quantum yield. Hence, halide perovskites have great potentials for applications in the new generation of light emitting devices. It has been demonstrated that the performances of LEDs could be greatly improved due to the QCE in semiconductors. Here, we take QCE in $CsPbBr_3$ as an example to represent QCE in all-inorganic halide perovskites. Firstly, the exciton Bohr diameter of $CsPbBr_3$ was evaluated to be about 7 nm based on DFT calculations, which is in good agreement with previous study [11], (seen in Supplementary information) i.e., QCE becomes important in $CsPbBr_3$ if its size or thickness is comparable to 7 nm, as shown in Fig. 1.

Then, the cubic $CsPbBr_3$ nanoplates samples with different thicknesses and sizes were prepared using the hot injection method. The prepared $CsPbBr_3$ nanoplates with thicknesses of 1.8, 3.0 and 30 nm exhibit strong (002) diffraction peaks according to the XRD patterns, as shown in Fig. 2. These thicknesses correspond to 3, 5 and more than 50 layers, respectively (the interplanar spacing of (002) plane is 0.58 nm). We can see that the nanoplates with thinner thicknesses stand vertically and arrange regularly due to the high concentration and residual ligands while larger sheets assemble flat on the Cu grid.

Band gap and exciton binding energy evolutions with 2D thickness reductions

Numerous previous studies showed that the blue shift of

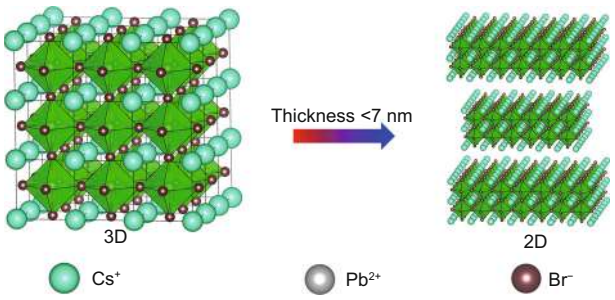

Figure 1 Excitons in bulk $CsPbBr_3$ have a diameter of about 7 nm (according to the DFT simulations). 2D structures are defined as material sizes reduced and comparable with about 7 nm in one dimension.

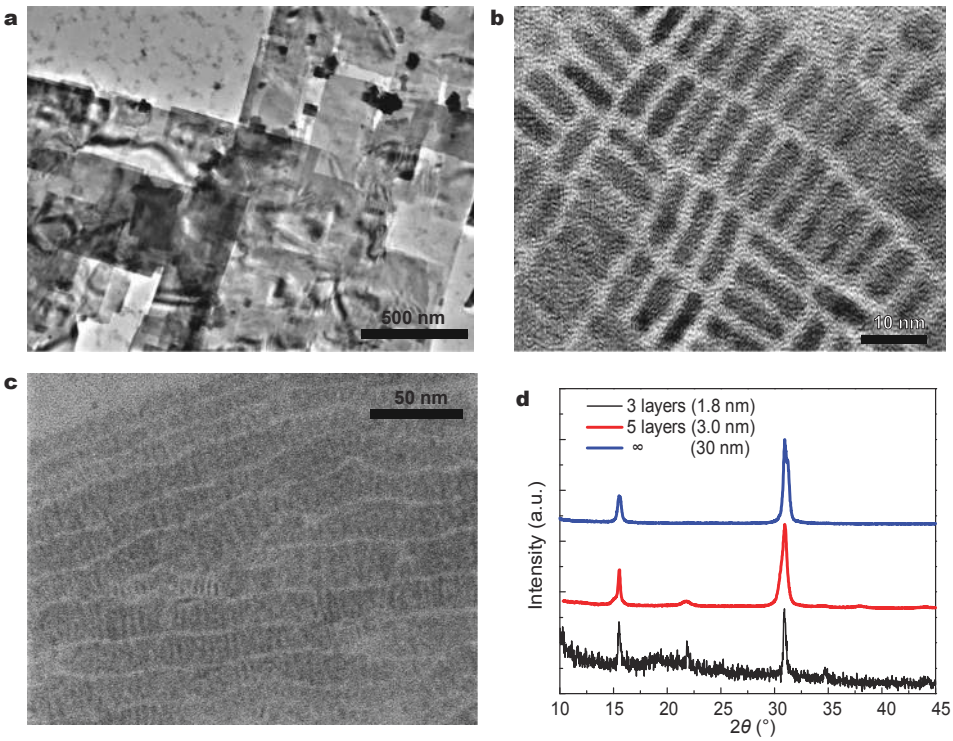

Figure 2 (a–c) Transmission electron microscopy (TEM) image of 30, 3.0, and 1.8 nm thickness $CsPbBr_3$ nanoplates, respectively. (d) XRD patterns of different thickness $CsPbBr_3$ nanoplates.

absorption and PL spectra is a basic characteristics of QCE [7,15]. Fig. 3 shows that the peaks of absorption and PL spectra of $CsPbBr_3$ are also exceptionally dependent on the size of nanoplates. In nanoplates, the gradually increasing QCE results in a significant blue shift of the excitonic absorption peaks from 2.42 eV to 3.00 eV by decreasing the thickness from 30 to 1.8 nm. Meanwhile, the excitonic absorption peaks become more dominant while decreasing the thickness, which implies a significant increase of exciton binding energy [31]. In another aspect, the absorption step is a very important feature in 2D materials, which is caused by discrete energy levels. The steps would become increasingly close with the thickness increasing, until they merge into the bulk absorption, which is continuous and has no steps. We see from Fig. 3b, c that the nanoplate absorptions are indeed a series of steps, and the steps in 3.0 nm thickness nanoplate absorption become closer compared with that in 1.8 nm thickness absorption.

PL is another essential evidence to evaluate the QCE. For bulk $CsPbBr_3$, the PL peak at about 522 nm (corresponding to 2.37 eV) is in good agreement with previous studies [7,9,12]. The blue shift in PL peaks from 467 to 437 nm in $CsPbBr_3$ nanoplates corresponds to the decreased thickness from 3.0 to 1.8 nm, indicating the strong QCE as the thickness decreases. This trend is in line with previous studies [18].

The bandgaps and exciton binding energy were extracted by fitting the absorption spectra with the following Equation (1) [32].

$$\begin{aligned}
&\text{3 D: } \alpha(\omega)=A\cdot\theta(\hbar\omega-E_g)\cdot\left(\frac{\pi e^{\pi x}}{\sinh(\pi x)}\right)\\
&+A\cdot E_b\sum_{i=1}^{\infty}\frac{4\pi}{i^3}\cdot\delta\left(\hbar\omega-E_g+\frac{E_b}{i^2}\right)\\
&\text{2 D: } \alpha(\omega)=B\cdot\theta(\hbar\omega-E_g)\cdot\left(\frac{\pi e^{\pi x}}{\cosh(\pi x)}\right)\\
&+B\cdot E_b\sum_{i=1}^{\infty}\frac{4\pi}{\left(i+\frac{1}{2}\right)^3}\cdot\delta\left(\hbar\omega-E_g+\frac{E_b}{\left(i+\frac{1}{2}\right)^2}\right),
\end{aligned}\tag{1}$$

where A is a constant related to the transition matrix element, B is a constant related to the transition matrix element and sample thickness. ω is the frequency of light, θ is the step function, E_g is the bandgap, x is defined as $E_b^{1/2}/(\hbar\omega-E_g)^{1/2}$, where E_b is the exciton binding energy, i is the principal quantum number and δ denotes the delta

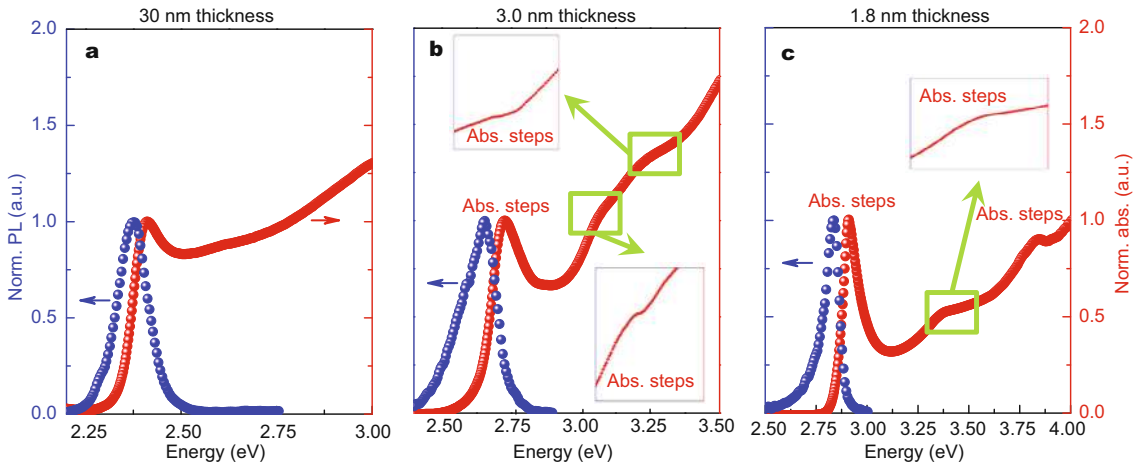

Figure 3 PL and absorption evolutions with 2D thickness. Blue dots are normalized PL spectra and red dots are normalized absorption spectra.

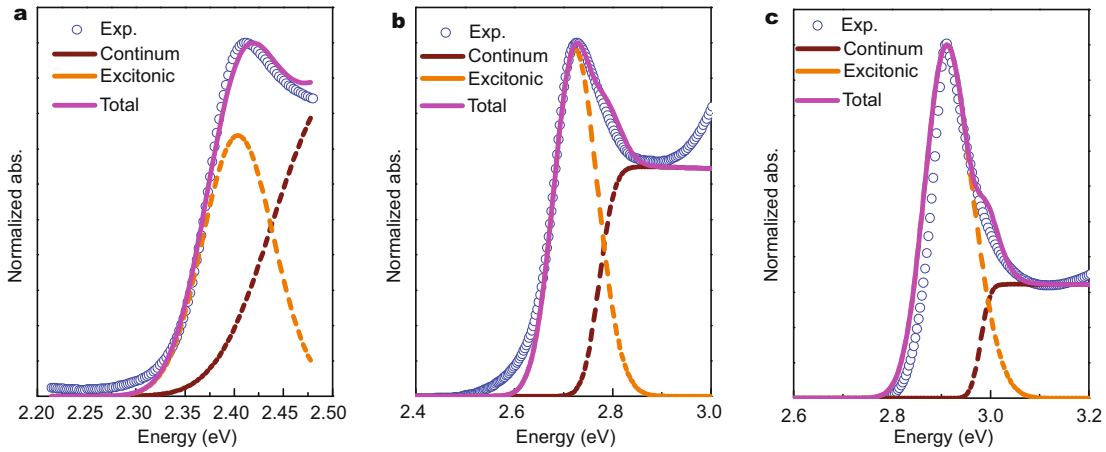

Figure 4 The absorption coefficient (blue circles) of (a) the 30 nm thickness, (b) the 3.0 nm thickness, and (c) the 1.8 nm thickness $CsPbBr_3$ perovskite nanoplates. The magnet line is the modelled absorption coefficient with excitonic (orange dash line) and continuum (wine dash line) components according to 3D and 2D Elliott models.

function. The first and second terms account for the continuum absorption corresponding to the bandgap and discrete absorption peak arising from the excitonic states, respectively. We modeled the absorption accounting for inhomogeneous broadening by convolving the step and delta function with a Gaussian function, as shown in Fig. 4. We found the least squares fitting values of E_b for 1.8, 3.0, and 30 nm thickness samples to be 180, 130, and 38 meV, respectively, with bandgap values of 2.98, 2.77, and 2.44 eV, respectively.

Temperature-dependent PL measurement of different thickness perovskites

Except for the regular absorption spectra and PL measurement, the temperature-dependent PL (TD-PL) spectrum is another powerful tool to analyze QCE, since band gap and exciton binding energy are affected by QCE [33], which can be obtained by fitting data extracted from emission energy *versus* temperature. TD-PL is shown in Fig. 5a–c for 30, 3.0, and 1.8 nm thickness, respectively. It is easy to find the common trend that increase in peak intensity, and decrease in FWHM as the temperature decreases. To observe the emission energy, integrated intensity, and FWHM of these samples clearly, we summarized the emission energy, integrated intensity, and FWHM as a function of temperature T or $1/T$ in Fig. 5d–f.

As shown in Fig. 5d, with temperature lowered, the emission energies of 30 nm thickness $CsPbBr_3$ nanoplates redshift. Such redshift was observed from $MAPbBr_3$ and other lead compound quantum dots (QDs) [34,35]. But

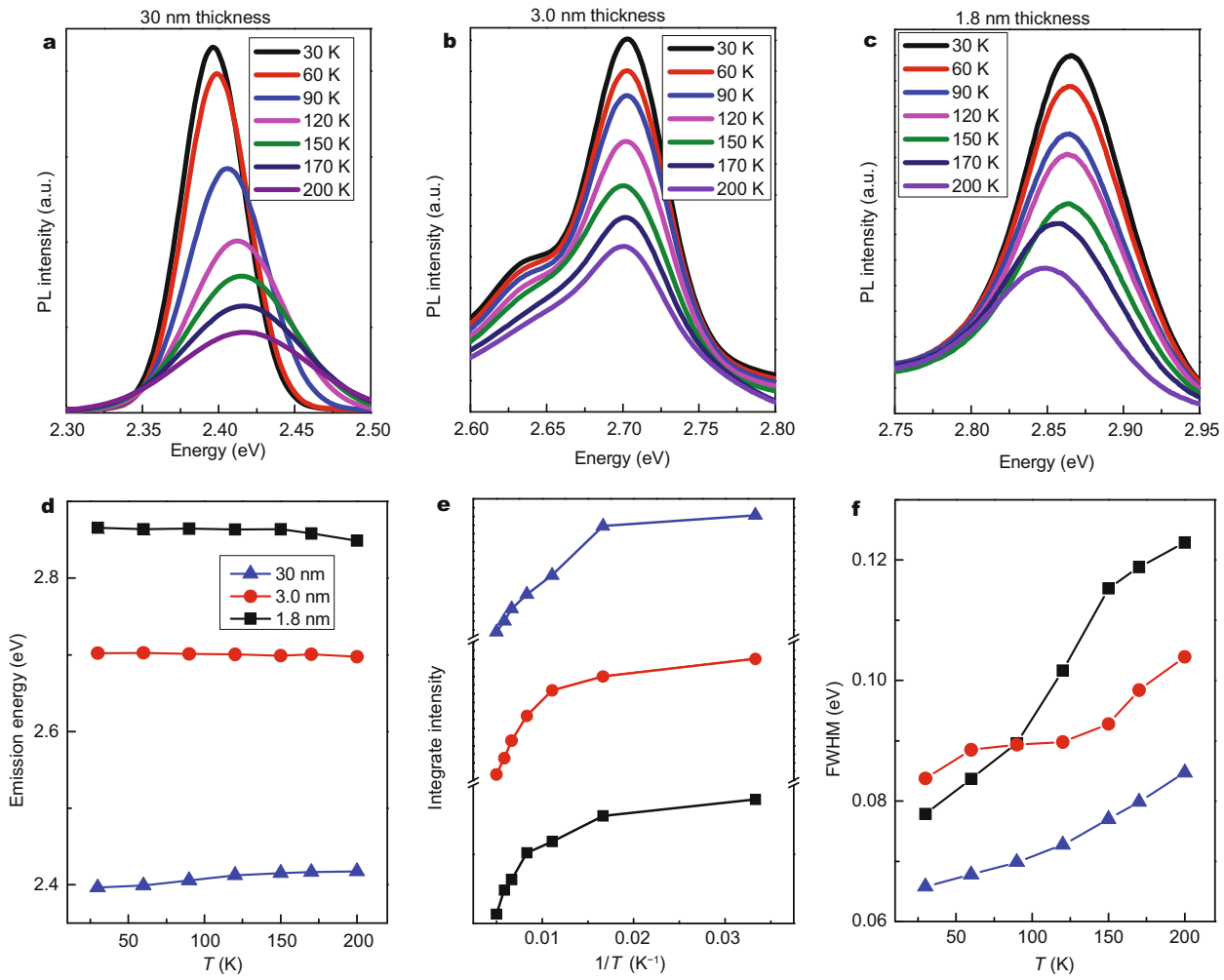

Figure 5 TD-PL of (a) 30 nm thickness, (b) 3.0 nm thickness, and (c) 1.8 nm thickness $CsPbBr_3$ nanoplates. (d) Emission energy, (e) integrated intensity and (f) FWHM of temperature-dependent PL from 30 to 200 K.

the emission energies for 3.0 nm nanoplates stay roughly at the same position no matter how the temperature changes. And the emission energies blueshift with the temperature decreasing, which is contrary to the bulk $CsPbBr_3$ and consistent with the Cd-based semiconductors [36,37]. In fact, this physical phenomenon is caused by the competition of the electronic properties anomalies caused by Pb 6s electrons [38] and Varshni effect. In other semiconductors, emission energy is fitted by the Varshni relation (2) [39],

$$E_g(T) = E_{g0} - \frac{\alpha T^2}{T+\beta}, \quad (2)$$

where E_{g0} is the band gap at 0 K, α is the temperature coefficient, and the value of β is close to the Debye temperature θ_D of the material. According this equation, the emission peaks should blueshift with temperature lowered. At the same time, the lattice constants a will contract, and this contraction gives rise to band gaps blueshift, as shown in Figs S1–3. In bulk systems, the electronic properties anomalies dominate the temperature-dependent emission behavior, while in 3 layer samples, the Varshni effect win the competition. As a result, these temperature-dependent emission behaviors show contrary trend.

Integrated intensity weakly decreases as the temperature below ~60 K, then nearly exponentially decreases above ~60 K for three samples due to activation of some non-radiative processes. This behavior suggests the presence of temperature-dependent nonradiative processes in our system. Integrated intensity is fitted by the standard expression for thermal quenching as a function of $1/T$

using the Equation (3) [40] as following,

$$I_{\text{int}}(T)=\frac{I_{\text{int}}(0)}{1+Ae^{-E_b/k_BT}}, \quad (3)$$

where $I_{\text{int}}(0)$ is the intensity at 0 K, A is a constant, E_b is the exciton binding energy, k_B is Boltzmann constant, and T is temperature. According to equation (3), the fitted E_bs are 36 meV, 135 mV, and 184 meV for 30, 3.0, and 1.8 nm thickness $CsPbBr_3$ samples, respectively. These data are in good agreement with DFT simulation and Elliott fitted results. The enhanced E_b indicates the process of thermal quenching slows down with material thickness decreases, and a strong quantum confine-ment effect exists in 2D halide perovskites.

CONCLUSIONS

In summary, we investigated and compared the QCE of $CsPbBr_3$ perovskite in 2D systems through the absorption, PL spectra and TD-PL characterization. Bandgaps E_g and exciton binding energy E_b are estimated by fitting the absorption spectra. Both E_g and E_b evolutions follow the common trend of QCE that the value increases as the thickness of nanoplates decreases. PL spectra show similar conclusion. However, the temperature dependence emission energy extracted from TD-PL shows a contrary shift in 1.8 nm nanoplates with respect to the 30 nm thickness samples. The interesting physical phenomena are still not understood. This work will help to understand the nature of the QCE in perovskite nanoplates, and help to design the all inorganic halide perovskites with desired optical properties.

Received 11 July 2017; accepted 3 August 2017; published online 5 September 2017

1 Wu Y, Wei Y, Huang Y, *et al.* Capping $CsPbBr_3$ with ZnO to improve performance and stability of perovskite memristors. Nano Res, 2017, 10: 1584–1594
2 Xing G, Mathews N, Sun S, *et al.* Long-range balanced electron- and hole-transport lengths in organic-inorganic $CH_3NH_3PbI_3$. Science, 2013, 342: 344–347
3 Stranks SD, Eperon GE, Grancini G, *et al.* Electron-hole diffusion lengths exceeding 1 micrometer in an organometal trihalide perovskite absorber. Science, 2013, 342: 341–344
4 Qin X, Dong H, Hu W. Green light-emitting diode from bromine based organic-inorganic halide perovskite. Sci China Mater, 2015, 58: 186–191
5 Tan ZK, Moghaddam RS, Lai ML, *et al.* Bright light-emitting diodes based on organometal halide perovskite. Nat Nanotech, 2014, 9: 687–692
6 Dong Y, Gu Y, Zou Y, *et al.* Improving all-inorganic perovskite photodetectors by preferred orientation and plasmonic effect. Small, 2016, 12: 5622–5632
7 Li X, Wu Y, Zhang S, *et al.* $CsPbX_3$ quantum dots for lighting and displays: room-temperature synthesis, photoluminescence superiorities, underlying origins and white light-emitting diodes. Adv Funct Mater, 2016, 26: 2435–2445
8 Li X, Yu D, Cao F, *et al.* Healing all-inorganic perovskite films via recyclable dissolution-recyrstallization for compact and smooth carrier channels of optoelectronic devices with high stability. Adv Funct Mater, 2016, 26: 5903–5912
9 Song J, Li J, Li X, *et al.* Quantum dot light-emitting diodes based on inorganic perovskite cesium lead halides ($CsPbX_3$). Adv Mater, 2015, 27: 7162–7167
10 Song J, Xu L, Li J, *et al.* Monolayer and few-layer all-inorganic perovskites as a new family of two-dimensional semiconductors for printable optoelectronic devices. Adv Mater, 2016, 28: 4861–4869
11 Wang Y, Li X, Zhao X, *et al.* Nonlinear absorption and low-threshold multiphoton pumped stimulated emission from all-inorganic perovskite nanocrystals. Nano Lett, 2016, 16: 448–453
12 Protesescu L, Yakunin S, Bodnarchuk MI, *et al.* Nanocrystals of cesium lead halide perovskites ($CsPbX_3$, X = Cl, Br, and I): novel optoelectronic materials showing bright emission with wide color gamut. Nano Lett, 2015, 15: 3692–3696
13 Ramasamy P, Lim DH, Kim B, *et al.* All-inorganic cesium lead halide perovskite nanocrystals for photodetector applications. Chem Commun, 2016, 52: 2067–2070
14 Li J, Xu L, Wang T, *et al.* 50-Fold EQE improvement up to 6.27% of solution-processed all-inorganic perovskite $CsPbBr_3$ QLEDs *via* surface ligand density control. Adv Mater, 2017, 29: 1603885
15 Dou L, Wong AB, Yu Y, *et al.* Atomically thin two-dimensional organic-inorganic hybrid perovskites. Science, 2015, 349: 1518–1521
16 Sichert JA, Tong Y, Mutz N, *et al.* Quantum size effect in organometal halide perovskite nanoplatelets. Nano Lett, 2015, 15: 6521–6527
17 Zhang Q, Su R, Liu X, *et al.* High-quality whispering-gallery-mode lasing from cesium lead halide perovskite nanoplatelets. Adv Funct Mater, 2016, 26: 6238–6245
18 Akkerman QA, Motti SG, Srimath Kandada AR, *et al.* Solution synthesis approach to colloidal cesium lead halide perovskite nanoplatelets with monolayer-level thickness control. J Am Chem Soc, 2016, 138: 1010–1016
19 Tsai H, Nie W, Blancon JC, *et al.* High-efficiency two-dimensional Ruddlesden–Popper perovskite solar cells. Nature, 2016, 536: 312–316
20 Ithurria S, Tessier MD, Mahler B, *et al.* Colloidal nanoplatelets with two-dimensional electronic structure. Nat Mater, 2011, 10: 936–941
21 Ha ST, Liu X, Zhang Q, *et al.* Synthesis of organic-inorganic lead halide perovskite nanoplatelets: towards high-performance perovskite solar cells and optoelectronic devices. Adv Optical Mater, 2014, 2: 838–844
22 Zhang Q, Ha ST, Liu X, *et al.* Room-temperature near-infrared high-Q perovskite whispering-gallery planar nanolasers. Nano Lett, 2014, 14: 5995–6001
23 Ling Y, Yuan Z, Tian Y, *et al.* Bright light-emitting diodes based on organometal halide perovskite nanoplatelets. Adv Mater, 2016, 28: 305–311
24 Bekenstein Y, Koscher BA, Eaton SW, *et al.* Highly luminescent colloidal nanoplates of perovskite cesium lead halide and their oriented assemblies. J Am Chem Soc, 2015, 137: 16008–16011

25 Jie D, Yan Q. Progress in organic-inorganic hybrid halide perovskite single crystal: growth techniques and applications. Sci China Mater, doi: 10.1007/s40843-017-9039-8
26 Cao D, Stoumpos C, Yokoyama T, *et al.* Thin films and solar cells based on semiconducting two-dimensional ruddlesden–popper $(CH_3(CH_2)_3NH_3)_2(CH_3NH_3)_{n-1}Sn_nI_{3n+1}$ perovskites. ACS Energy Lett, 2017, 2: 982–990
27 Huo C, Cai B, Yuan Z, *et al.* Two-dimensional metal halide perovskites: theory, synthesis, and optoelectronics. Small Methods, 2017, 1: 1600018
28 Chen S, Shi G. Two-dimensional materials for halide perovskite-based optoelectronic devices. Adv Mater
29 Xiong Y, Liu T, Jiang X, *et al.* N-type metal-oxide electron transport layer for mesoscopic perovskite solar cells. Sci China Mater, 2016, 59: 757–768
30 Ye L, Fan B, Zhang S, *et al.* Perovskite-polymer hybrid solar cells with near-infrared external quantum efficiency over 40%. Sci China Mater, 2015, 58: 953–960
31 Quantum Confinement Effect – Shodhganga. http://http://shodhganga.inflibnet.ac.in/bitstream/10603/23484/3/03.chapter%201.pdf
32 Excitons in bulk and two-dimensional semiconductors. http://homes.nano.aau.dk/tgp/PhD_Course/Excitons%20in%20bulk%20and%20low-dimensional%20semiconductors.pdf
33 Valerini D, Cretí A, Lomascolo M, *et al.* Temperature dependence of the photoluminescence properties of colloidal CdSe/ZnS core/shell quantum dots embedded in a polystyrene matrix. Phys Rev B, 2005, 71: 235409
34 Dey P, Paul J, Bylsma J, *et al.* Origin of the temperature dependence of the band gap of PbS and PbSe quantum dots. Solid State Commun, 2013, 165: 49–54
35 Zhao YS, Fu H, Peng A, *et al.* Low-dimensional nanomaterials based on small organic molecules: preparation and optoelectronic properties. Adv Mater, 2008, 20: 2859–2876
36 Jing P, Zheng J, Ikezawa M, *et al.* Temperature-dependent photoluminescence of CdSe-core CdS/CdZnS/ZnS-multishell quantum dots. J Phys Chem C, 2009, 113: 13545–13550
37 Varshni YP. Temperature dependence of the energy gap in semiconductors. Physica, 1967, 34: 149–154
38 Wei S, Zunger A. Electronic and Structural anomalies in lead chalcogenides. Phys Rev B, 1997, 55: 13605
39 M Ueta, H Kanzaki, K Kobayashi, Y Toyozawa, E Hanamura. Exciton-phonon processes in silver halides. In Excitonic Processes in Solids. Berlin: Springer Berlin Heidelberg, 1986, 309-369
40 Stoumpos CC, Malliakas CD, Peters JA, *et al.* Crystal growth of the perovskite semiconductor $CsPbBr_3$: a new material for high-energy radiation detection. Cryst Growth Des, 2013, 13: 2722–2727

Acknowledgements This work was supported by the National Basic Research Program of China (2014CB931702), the National Key Research and Development Program of China (2016YFB0401701), the National Natural Science Foundation of China (NSFC 51572128 and 21403109), NSFC-RGC (5151101197), the Natural Science Foundation of Jiangsu Province (BK20160827), China Postdoctoral Science Foundation (2016M590455), the Fundamental Research Funds for the Central Universities (30915012205 and 30916015106), and the Priority Academic Program Development of Jiangsu Higher Education Institutions (PAPD).

Author contributions Cai B and Zeng H designed the experiments; Cai B, and Xie M performed the DFT calculations; Moussab H, and Luigi C calculated the exciton binding energy and Bohr radius; Li X, and Cao F prepared the samples; Li J, and Song J conducted the measurement and characterization; Gu Y fitted the absorption spectra *via* Elliott models; Cai B, Li X, and Gu Y analyzed the results and wrote the manuscript; Moussab H, Zhang S, and Zeng H polished English. All authors contributed to the general discussion.

Conflict of interest The authors declare that they have no conflict of interest.

Supplementary information The supporting data are available in the online version of this paper.

Bo Cai received his bachelor degree in materials science and engineer from Nanjing University of Science and Technology in 2013. Now, he is a PhD candidate in Prof. Zeng's group. His current research interest is perovskite DFT simulations.

Xiaoming Li received his PhD degree in material science from Nanjing University of Aeronautics and Astronautics in 2017. Now, he is a research member in Prof. Zeng's group. His current research interests include all-inorganic halide perovskites and their optoelectronic applications.

Yu Gu received his PhD degree from Clemson University, USA in 2014. Now, he is an associate professor in Prof. Zeng's group. His current research interest is optoelectronic device simulation.

Haibo Zeng received his PhD degree from the Institute of Solid States Physics, Chinese Academy of Sciences in 2006. Now he is the leader of MIIT Key Laboratory of Advanced Display Materials and Devices, Institute of Optoelectronics & Nanomaterials. His current research interests are low-dimensional semiconductor optoelectronics including 2D materials (simulations and experiments) and QDs (synthesis, optics, photodetectors and LEDs).

全无机卤素钙钛矿中的量子限域效应

蔡波[1†], 李晓明[1†], 顾宇[1†], Moussab Harb[2], 李建海[1], 谢美秋[1], 曹菲[1], 宋继中[1], 张胜利[1], Luigi Cavallo[2], 曾海波[1*]

摘要 当半导体材料尺寸缩小到与激子尺寸相当时, 量子限域效应会在对应的低维材料中诱导出不同的物理行为. 本文以$CsPbBr_3$为例, 报道了在全无机钙钛矿纳米片中的量子限域效应. 根据DFT理论模拟可知, 当$CsPbBr_3$材料减薄至7纳米左右时, 该效应导致该材料的光吸收和光致发光光谱的峰位蓝移, 且样品越薄, 峰位蓝移现象越明显. 该效应也会导致激子束缚能随着材料厚度的减薄而显著增大. 同时, 变温光致发光光谱的光强-温度与半高宽-温度函数都显示出厚度越薄量子限域效应越强的趋势. 本文揭示了二维全无机卤化物钙钛矿的量子限域效应, 可为设计全无机卤化物钙钛矿光电器件提供参考依据.